SCIENCE CHINA
Earth Sciences

• RESEARCH PAPER •

doi: 10.1007/s11430-010-4101-1

Three Gorges Dam stability monitoring with time-series InSAR image analysis

WANG Teng[1,2*], PERISSIN Daniele[3,2], ROCCA Fabio[2] & LIAO Ming-Sheng[1]

[1] *State Key Laboratory of Information Engineering in Surveying, Mapping and Remote Sensing, Wuhan University, Wuhan 430079, China;*
[2] *Dipartimento di Elettronica e Informazione, Politecnico di Milano, Milan 20133, Italy;*
[3] *Institute of Space and Earth Information Science, Chinese University of Hong Kong, Hong Kong, China*

Received September 6, 2009; accepted May 25, 2010

In this paper, we carried out a combination of permanent scatterer and quasi permanent scatterer time-series InSAR image analyses to extract geometric information over the area of the Three Gorges Dam. For the first time, we measured and analyzed the deformation of the Three Gorges Dam and its surrounding area using 40 SAR images acquired from 2003 to 2008. Our results indicate that the temporal deformation of the left part of the dam has ceased and that the deformation of the dam was influenced by the changing level of the Yangtze River. Seasonal deformation due to varying temperature is also observed. The obtained results agree well with the published results of the Three Gorges Dam deformation obtained by employing conventional survey methods. We also found that there is an area of abnormal subsidence near Zigui County. This paper demonstrates the potential of time-series InSAR image analysis in the monitoring of dam stability and measurement of subsidence.

Three Gorges Project, deformation monitoring, InSAR, permanent scatterer analysis

Citation: Wang T, Perissin D, Rocca F, et al. Three Gorges Dam stability monitoring with time-series InSAR image analysis. Sci China Earth Sci, 2010, doi: 10.1007/s11430-010-4101-1

China is presently in an era of rapid urbanization and infrastructure construction, and many projects have been constructed and begun operation. The Three Gorges Project (TGP), the largest hydroelectric project in the world, is one of the most significant recent construction projects in China. The three main functions of the TGP, namely, flood control, power generation and navigational assistance, have brought about remarkable economic, social and environmental benefits. With completion of the dam, a 660 km long reservoir was formed. Owing to the high pressure of the reservoir on the riverbed and water infiltration, there is potential crust instability along the river. The crustal structure and dynamic variations in the gravity field in this area have been studied after the river was dammed [1–3]. Besides the rising water, the weight of the dam itself has applied substantial pressure on the riverbed crust and caused deformation.

Indeed, deformation is unavoidable for any dam. Although small deformations are acceptable, when the deformation reaches a certain level, there is great risk to the dam and obviously the downriver areas [4]. Since the safety of the Three Gorges Dam relates to millions of people living on the downriver plain, monitoring of stability is important [5].

The main part of the TGP is a concrete gravity dam, for which there are two types of deformation. One is vertical subsidence caused by the weight of the dam itself, and it is usually monitored using high-precision leveling. The other type of deformation is caused by the pressure of the upriver water and is perpendicular to the main axis of the dam.

*Corresponding author (email: wang.teng@gmail.com)

Monitoring this type of deformation is complicated, and the surroundings have to be theoretically considered. Conventional methods include the collimation line method, triangular mesh intersection method, and the triangulation network method [4]. In addition, a differential global positioning system (GPS) technique has been applied to the monitoring of the horizontal deformation of a dam [6].

Since the Three Gorges Dam was built in a highly stable basin, dam deformation occurs at the millimeter level, and thus, high-precision deformation measurement methods are needed [5]. Although nowadays, dam deformation monitoring systems are capable of making high-precision measurements with a certain spatial density, no matter which survey method is employed, it is necessary to install and maintain monitoring stations. Therefore, it is difficult to increase the number of measurement points. Furthermore, some survey methods (e.g., leveling) are time consuming in terms of obtaining measurement data. In general, conventional dam deformation methods are able to acquire high-precision measurements; however, high financial and labor costs are unavoidable.

As coherent imaging radar working in the microwave frequency, Synthetic Aperture Radar (SAR) allows us to acquire data over a wide area under all conditions (i.e., day or night and for any weather). The applications of SAR are significant in cloudy areas, where it is difficult to acquire data through optical remote sensing [7]. Interferometric SAR (InSAR) is one of the most important applications of SAR. The InSAR technique takes advantage of coherent phases of SAR echoes to extract precise geometric information; the basic principle is to inversely obtain the terrain elevation from the phase differences and orbital parameters of two SAR images taken while illuminating the same surface [7–12]. Moreover, when the topography is available and can be subtracted from the corresponding interferogram, the residual phases represent the deformation of the illuminated ground. As the technique is based on InSAR, it is referred to as differential InSAR (D-InSAR). D-InSAR is able to obtain high-spatial density centimeter-level deformation measurements. The D-InSAR technique has been successfully applied to the monitoring of coseismic ground deformation, volcanic deformation and mining deformation [13–17].

The conventional D-InSAR technique is suitable for obtaining large ground deformation over a wide area; however, it cannot reach the level of precision required for the monitoring of dam deformation. There are four reasons for this: 1) the wavenumber shift caused by normal baseline dispersion reduces the interferogram coherence (i.e., there is geometric decorrelation) [18], 2) there is temporal decorrelation due to changes in the ground physical characteristics, 3) there is an atmospheric phase screen (APS) difference between master and slave images [19, 20], and 4) there are system noise, processing errors and other errors.

To overcome the above limitations of D-InSAR, the permanent scatterer (PS)-InSAR technique was proposed and has since became the core concept in precisely measuring earth deformation from a time series of SAR images [21–23]. Instead of extracting information from each pixel of an interferogram, PS-InSAR firstly identifies certain artificial or natural point-like stable reflectors; i.e., PSs from a long time series of interferometric SAR images. For a target on the ground to be a PS, three conditions have to be fulfilled: 1) the target has to remain physically stable during the time series, 2) the target has to be sufficiently small (smaller than the SAR resolution cell) to avoid geometric decorrelation and 3) the backscattering coefficient of the target has to be much higher than the coefficients of other targets within the SAR resolution cell [21, 22, 24]. From a sparse graph of PSs, one can separate topography, deformation, and APS phases according to their different spatial and temporal characteristics. Finally, high-accuracy deformation measurements can be obtained [25, 26]. The PS-InSAR technique takes advantage of 20-year archived SAR images and has been successfully applied in earth deformation monitoring, particularly urban subsidence monitoring [27–29]. Meanwhile, research groups have developed several open-source scientific PS systems that are widely used in the earth science community [30, 31].

The PS-InSAR technique is the first to allow millimeter-level deformation monitoring through a space-borne Earth-observation dataset, and its contributions are undoubted. However, because of the strict PS selection requirements, information hidden in the distributed targets that partially maintain coherence in both temporal and spatial dimensions has to be disregarded. Therefore, applications of the PS technique are limited in areas where few stable point-like targets are available. By loosening the PS restrictions and applying new spatial and temporal filtering techniques, new methods that extract topography and deformation information from a small baseline dataset have been proposed [31–33]. We also presented the quasi-PS (QPS) technique by considering different interferometric combinations in time-series SAR images[1)]. All these techniques expand the PS technique into geological fields such as the monitoring of landslides and the study of fault deformation [31, 33–35], allowing us to monitor deformation over the area of the Three Gorges Dam.

Since 2003, the Advanced Synthetic Aperture Radar on board the Envisat satellite of the European Space Agency (ESA) has been acquiring SAR images over the area of the Three Gorges Dam (the shortest revisiting time is 35 days).

1) Perissin D, Wang T. Repeat-Pass SAR Interferometry with Partially Coherent Targets. Submitted to IEEE Transactions on Geoscience and Remote Sensing, 2010

With the completion of the TGP in 2009, we try to extract and analyze the deformation of the Three Gorges Dam and its surroundings from time-series SAR images in this paper. Since there are various types of targets in this area, we propose a combination of PS and QPS analyses to measure the deformation of the Three Gorges Dam from space-borne Earth-observation data. The deformation trends that we obtained closely fit those of previous studies obtained by employing conventional survey methods [36], and show the potential of using time-series SAR images in monitoring dam stability and ground deformation at dam sites.

1 Time-series SAR image analysis techniques

We first briefly recall the basic principle and algorithms of the PS technique, and then present our new QPS algorithm. The target distribution of the Three Gorges Dam site is complicated, and there are both stable point-like artificial targets and distributed targets such as bare land and rocks. In this paper, we carry out both QPS and PS analyses; therefore, a reasonable number of measurements can be obtained for the QPS analysis and the deformation can be measured with high accuracy in the PS analysis.

1.1 PS technique

Let us denote with s_i the i-th complex SAR image (where $i = 1, \cdots, N$). The interferogram between images i and k can thus be expressed as $I^{i,k} = s_i \cdot s_k^*$ (where * indicates the complex conjugate operator). Taking target p_0 as a reference point, the interferometric phase $\Delta\phi_{p,p_0}^{i,k} = \angle I_{p,p_0}^{i,k}$ of target p depends on its geometrical location as well as its displacement, atmospheric disturbance and noise. In particular, the terms that depend on the target height difference $\Delta h_{p,p_0}$ and linear deformation difference $\Delta v_{p,p_0}$ are expressed respectively as [9]

$$\Delta\phi_{H,p,p_0}^{i,k} = \frac{4\pi}{\lambda}\frac{1}{R\sin\theta}\Delta h_{p,p_0} B_n^{i,k}, \tag{1}$$

$$\Delta\phi_{D,p,p_0}^{i,k} = \frac{4\pi}{\lambda}\Delta v_{p,p_0} B_t^{i,k}, \tag{2}$$

where $\Delta h_{p,p_0}$ and $\Delta v_{p,p_0}$ are the height and deformation differences between p and p_0, $B_n^{i,k}$ is the interferometric normal baseline, $B_t^{i,k}$ is the temporal baseline, λ is the radar wavelength, R is the sensor-target distance of target p, and θ is the viewing angle of the SAR sensor.

In the original PS technique, the height and deformation of the targets are usually estimated by maximizing the temporal coherence ξ_p [21]:

$$(\Delta\hat{h}_p, \Delta\hat{v}_p) = \arg\{\max(|\xi_p|)\}, \tag{3}$$

where

$$\xi_p = \frac{1}{M}\sum_{i,k} e^{j(\Delta\phi_p^{i,k} - \Delta\phi_{H,p}^{i,k} - \Delta\phi_{D,p}^{i,k})}. \tag{4}$$

Here, $\Delta\phi_p^{i,k}$ is the acquired interferometric phase (after flattening and external topographic correction), $\Delta\phi_{H,p}^{i,k}$ is the topography-related phase in eq. (1), and $\Delta\phi_{D,p}^{i,k}$ is the deformation-related phase in eq. (2).

The temporal coherence estimate $\hat{\xi}_p$ can be approximated as a function of phase dispersion: $\hat{\xi}_p \simeq e^{-\delta_\phi^2/2}$. Finally, the dispersions of the PS-estimated height and deformation velocity ($\delta_{\Delta h}^2$ and $\delta_{\Delta v}^2$) can be expressed approximately as functions of the phase dispersion, δ_ϕ^2, interferometric normal and temporal baselines ($\delta_{B_n}^2$ and δ_{Bt}^2), and the number of interferograms M [23]:

$$\delta_{\Delta h}^2 \simeq \left(\frac{\lambda R\sin\theta}{4\pi}\right)^2 \frac{\delta_\phi^2}{M\delta_{B_n}^2}, \tag{5}$$

$$\delta_{\Delta v}^2 \simeq \left(\frac{\lambda}{4\pi}\right)^2 \frac{\delta_\phi^2}{M\delta_{Bt}^2}. \tag{6}$$

Eqs. (5) and (6) show that the accuracies of the height and deformation velocity estimates obtained by employing the PS technique are functions of the temporal coherence and baseline distribution. The model is independent of the interferometric combination, and thus the expressions are useful for all time-series InSAR analysis techniques.

1.2 QPS technique

If we use the concepts of the vertices and edges from graph theory to represent time-series SAR images and interferometric connections, the original PS and StaMPS techniques are represented by star-like graphs; i.e., all the time-series SAR images are coregistered with a single master image. There are two benefits in using this interferometric configuration: 1) it is possible to carry out phase unwrapping in the temporal dimension [31] and 2) with higher $\delta_{\Delta h}^2$ and $\delta_{\Delta v}^2$ in eqs. (5) and (6), estimates of higher accuracy can be obtained. However, as discussed at the beginning of this section, the information contained in the distributed and decorrelated targets cannot be extracted from the single-master interferometric configuration. To continue studying the time-series SAR image combination with graph theory, we have to find weight to index interfero-

grams with different qualities to optimize the interferometric combination.

Naturally, coherence is the most commonly used index in InSAR literature. Coherence is a measure of the similarity of complex InSAR echoes, whose mathematical definition is [36]

$$\gamma = \frac{E\{s_i \cdot s_k^*\}}{\sqrt{E\{|s_i|^2 \cdot |s_k|^2\}}}. \tag{7}$$

Here, $E\{\cdot\}$ is the mathematical expectation and s_i and s_k are an interferometric image pair. Since the mathematical expectation of radar signals is not attainable in practice, coherence is usually estimated by spatially averaging the radar echoes in a moving window:

$$\hat{\gamma} = \frac{\sum_{n=1}^{L} s_{i,n} s_{k,n}^* \cdot \mathrm{e}^{-j\phi(n)}}{\sqrt{\sum_{n=1}^{L} |s_{i,n}|^2} \sqrt{\sum_{n=1}^{L} |s_{k,n}|^2}}. \tag{8}$$

Here, n represents the n-th pixel in the coherence estimation window. Since the topography-related phase in the coherent signal will under-bias the coherence estimates, an external digital elevation model (DEM) is usually used to remove this part of the interferometric phase $\phi(n)$ [37].

By calculating the coherence of all the interferometric combinations in the time-series SAR dataset (we usually use the average coherence of selected pixels as the approximate coherence values for the interferograms), we are able to use $1-\hat{\gamma}_{i,k}$ as the index of the connections between SAR images i and k. The minimum spanning tree (MST) algorithm [38] is then proposed to obtain the optimum interferometric subset $\{I_{i,k}\}$:

$$\{I_{i,k}\} = \min \sum (1-\hat{\gamma}_{i,k}). \tag{9}$$

On the basis of the MST-generalized interferometric configuration, the QPS technique differs from the PS technique in both temporal and spatial dimensions. In the temporal dimension, since the interferograms in the QPS image configuration contain also partially coherent targets, $|\hat{\gamma}_p^{i,k}|$ is used as the weight in eq. (4), and we obtain the QPS temporal coherence definition:

$$\xi_p = \frac{\sum_{(i,k)} \left|\hat{\gamma}_p^{i,k}\right| \mathrm{e}^{j(\Delta\phi_p^{i,k} - \Delta\phi_{H,p}^{i,k} - \Delta\phi_{D,p}^{i,k})}}{\sum_{(i,k)} \left|\hat{\gamma}_p^{i,k}\right|}. \tag{10}$$

During the procedures of maximizing ξ_p, when a target shows low coherence in some interferograms, the interferometric phase cannot influence other measurements [39].

In the spatial dimension, considering the baseline decorrelation [40], spatial filtering techniques that are seldom used in the PS technique have to be applied to all interferograms to extract more information from the time-series InSAR dataset.

The QPS technique maximizes the temporal coherence by estimating the elevation and deformation-related phases from a selected subset of interferograms for time-series SAR images. The technique modifies the interferometric combination strategy of the PS technique; nevertheless, it can be easily inserted in the processing chain described in the literature without requiring remarkable changes. Moreover, the same theoretical accuracy of the PS technique can be used to validate the QPS estimates.

1.3 Combination of PS and QPS analyses

The QPS technique is proposed to resolve the problem of how to increase the number of measurement points in the time-series InSAR dataset in the extra-urban areas where there are not enough stable point-like targets to employ the PS technique. However, the shortcoming is that the accuracy of the points extracted using the QPS technique is limited. There are two reasons for this. One reason is that the interferograms with high coherence are limited to image pairs with short temporal and spatial baselines, and the low $\delta_{B_n}^2$ and $\delta_{B_t}^2$ restrict the measurement accuracy. The other reason is that the spatial filtering reduces the accuracy of information extraction.

The PS and QPS techniques are quite complementary. In urban areas where many artificial stable targets can be identified, the PS technique can achieve highly accurate results. On the other hand, in extra-urban areas where distributed and decorrelated targets dominate the reflected signal, the QPS technique is more flexible.

The test site of this paper is around the Three Gorges Dam, where there are not only stable point-like targets on the body of the dam, but also many partially coherent targets present during the construction of the dam. The large number of distributed targets makes it difficult to obtain enough PSs in this area. Although the QPS technique can increase the number of measurement points, the accuracy of the results is insufficient for dam stability monitoring because of the short temporal baseline image pairs.

For the situation at hand, it is impossible to obtain a satisfactory result by employing either the PS or QPS technique alone. Moreover, since the Three Gorges Dam is a huge artificial target, the terrain of the entire dam site changed significantly, and thus, it is difficult to estimate the elevation without an up-to-date DEM. Therefore, in the area of the Three Gorges Dam, we propose a combination of QPS and PS analyses as the solution. First, we implement the QPS technique to measure the elevation and deformation trends of the detected targets, and then the QPS results

are used as the initial values in PS processing. Finally, we interpret the measured deformation of the dam using hydrological data published by the TGP Corporation.

2 Test site and dataset

The Three Gorges Dam is located in the town of San Douping, which is 40 km from Yichang, Hubei Province. There was a small island in the middle of the Yangtze (Zhongbao Island) before the construction of the dam. The presence of the island was helpful in constructing the dam in three different parts. The geologic basin consists of granite that has high compressive resistance. The lithesome is well cemented and no fault crevice has developed. With very weak hydraulic permeability, the geologic environment is suitable for constructing a concrete dam. The weathering crust is thick (20–40 m) along the mountain bodies. Earthquake activity around the dam is low in intensity and frequency [41].

The different parts of the dam are shown in Figure 1 with its surroundings; there is bare land, hills, the body of the dam, ship locks and other types of natural and artificial targets. The main part of the TGP consists of the dam, hydrological generator plants and navigation instruments. The body of the dam is 2355 m in length and has a highest elevation of 185 m. The width of the dam is 115 m at the base and 40 m at the top. The spillway is in the middle of the dam where the main river canal was. The 23 sluice gates installed at the base of the dam are used to control the capacity of the upstream reservoir and to wash alluvial sands to the downstream area. The power plants, flanking the spillway (on left and right riverbanks), accommodate a total of 26 sets of hydrologic turbine generators. The first generator in the left-riverbank plant house began operation in 2003, and the construction of the right-riverbank plant house was finished in 2008. The navigational part of the Three Gorges Project was built on the left riverbank and consists of permanent ship locks and a ship lift.

In this paper, 40 scenes of Evisat ASAR images, acquired from August 2003 to April 2008, are used as the data source. The wavelength of this SAR sensor is 5.62 cm, and the spatial resolutions are about 5 m in azimuth and 25 m in range. The hydrologic data published by the TGP Corporation are also referenced in this work. Figure 2 shows the image acquisition date and the corresponding upriver water

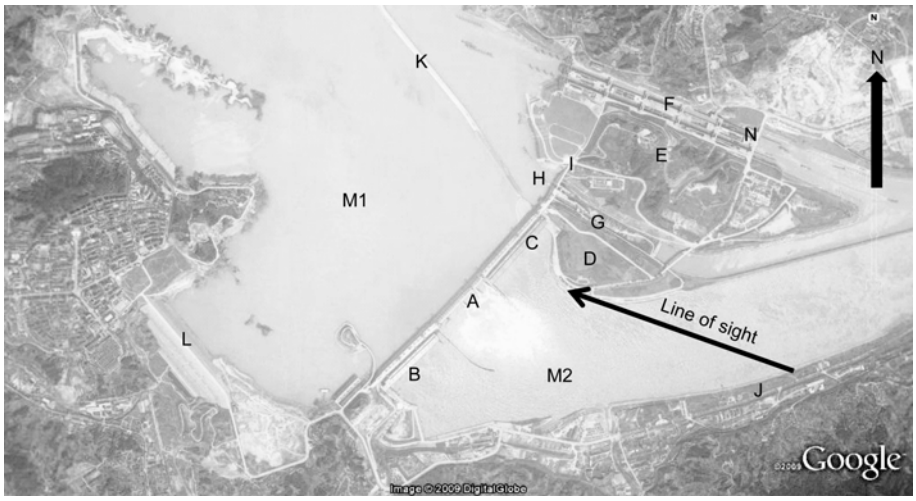

Figure 1 Studied area over the Three Gorge Dam site. The optical image is taken from Google Earth software. A, spillway; B, right planthouse; C, left planthouse; D, dam lookout; E, Tanziling Hill; F, permanent ship lock; G, temporal ship lock; H, ship lift; I, platform at 185 m elevation; J, memorial park; K, dyke; L, dyke; M1, the Yangtze River (upriver); M2, the Yangtze River (downriver); N, ship lock lookout.

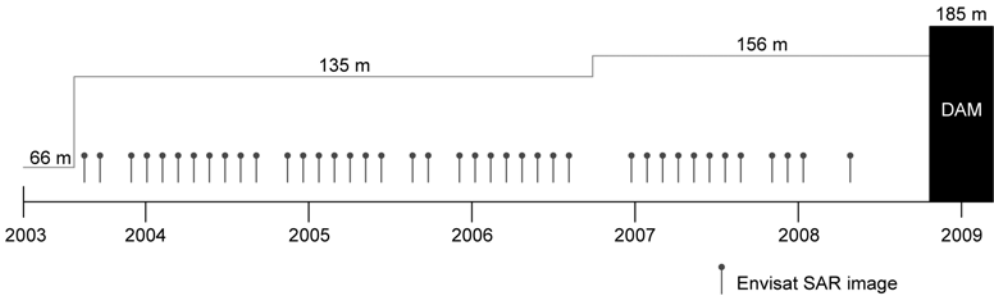

Figure 2 Water levels during the Envisat data acquisition period.

level. From (Figure 2), we find that before the first image was acquired in 2003, the water level rose nearly 90 m, and in the middle of 2006, the water level rose about 20 m. In the following discussions, we analyze the effect of the water level on the stability of the dam from the time-series InSAR results.

Figure 3 shows the incoherent mean amplitude values of the 40 SAR images. Because the line of sight is towards the downriver part of the dam (see Figure 1), the power plants, spillway and body of the dam can be observed by the satellite. The right part of the dam (part B in Figures 1 and 3) was under construction during the time span of our dataset. As a consequence, the mean amplitude image represents targets on the construction site; the cofferdam was dismantled in June 2006 but can still be seen in Figure 3.

3 Results and discussion

3.1 Interferometric combination

Before the time-series analysis, all 40 SAR images are oversampled in the range dimension with factor 2 and co-registered with the master image, which was acquired on 25 September 2005. After the procedures, 40 SAR images with the same grid as the master image are generalized with 12 m resolution in range and 5 m resolution in azimuth.

According to the previous discussions, the interferometric combination methods of the PS and QPS techniques are different. Figure 4(a) and (b) are the graphs formed by the SAR images (as vertices) and interferograms (edges). The graph representing the PS technique is star-like. The colors of the edges in Figure 4(b) represent the coherence of each interferogram. The interferometric graph generalized by the MST algorithm can achieve the optimum interferometric combination; moreover, the tree characteristics in graph theory ensure the graph matrix is invertible. Thus, topography and deformation parameters can be easily inverted from all the interferograms. The standard deviation of the normal and temporal baselines of PS and QPS interferogram combinations were $\delta_{PSBn} = 258$ m, $\delta_{PSB_t} = 512$ day, $\delta_{QPSBn} =$ 58 m, $\delta_{PSB_t} = 210$ day, respectively. With the interferograms, the pixels with average coherence greater than 0.25 were selected as the target candidates [28], from which the final measurement targets are selected.

3.2 Topography and deformation measurements

In the time-series InSAR analysis, a DEM derived from Shuttle Radar Topography Mission (SRTM) data is usually used to obtain initial topographic parameters. However, since the mission was carried out in 2000, at the very beginning of dam construction, the SRTM DEM does not represent the up-to-date topography of our test site. Therefore, in this paper, we first obtain the DEM of our test site by employing the QPS technique. As shown in Figure 5, high temporal coherence is achieved using the QPS algorithm. The left and top parts of the dam show very high coherence owing to temporal stability and strong reflectivity. Moreover, except for vegetated areas, stable distributed targets such as Tanziling Hill and the upriver bank protection also show high coherence. On the contrary, the spillway, the navigation instruments and the right part of the dam show low temporal coherence. We leave discussion about the low-coherence areas to the next section. According to the normal and temporal baseline distributions, we set 0.75 as our threshold to select QPS points. Within the 60 km^2 area, 11,463 QPSs are detected, and their elevation and deformation are shown in Figures 6 and 7.

According to eq. (5), the accuracy of the obtained elevation of QPS points is better than 3 m. Since we cannot find any published topographic map of this area, the results are validated by investigating the results for some known locations: 1) the tail water platform of the left part of the dam is at 83.5 m, 2) the top of the left plant house is at 117.2 m, 3)

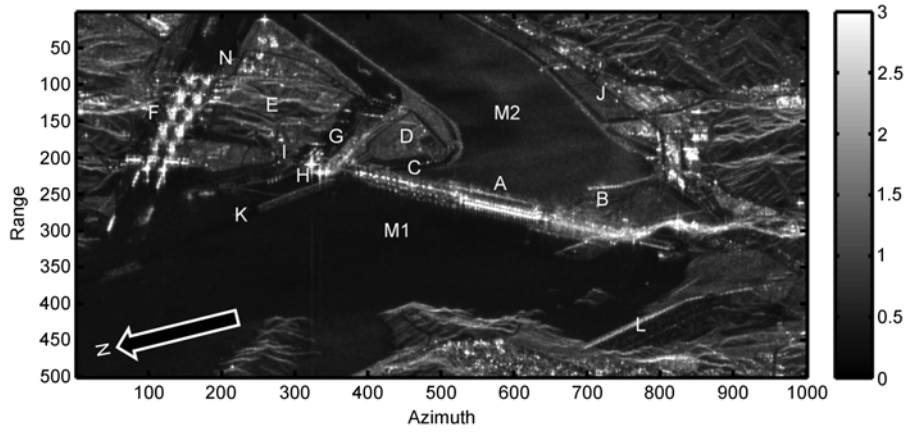

Figure 3 Incoherent amplitude mean of time-series SAR images. The letters match those from Figure 1.

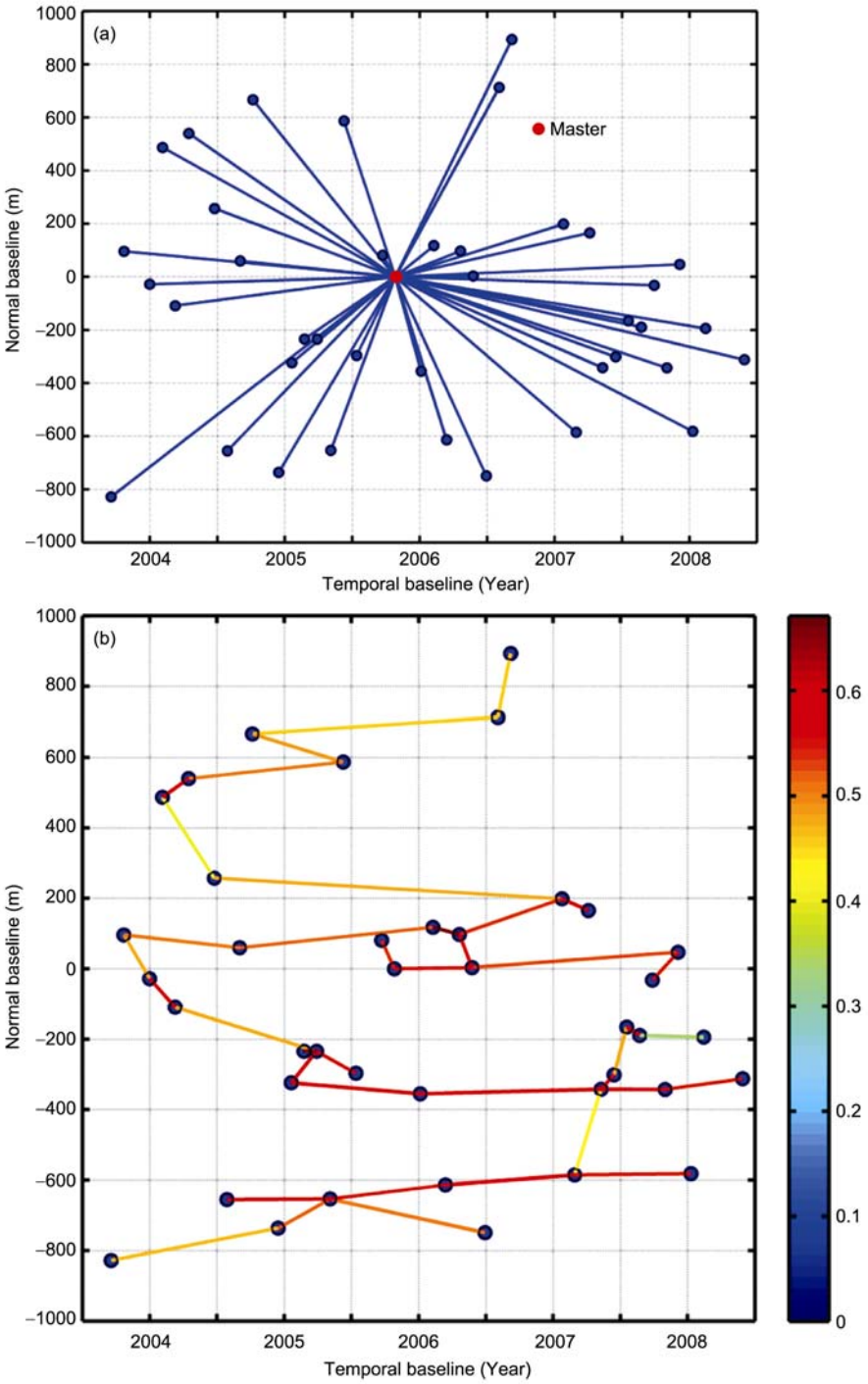

Figure 4 Different interferometric combinations. Each vertex indicates an SAR image acquired in a different temporal and spatial location. (a) PS image graph; the red point indicates the master image acquired on 25 September 2005. (b) QPS image graph; the color for each edge indicates the coherence of the interferogram that connects two SAR images.

the top of the dam is at 185 m, and 4) the spillway weir is at 158 m. The locations denoted by the letters in Figure 3 and the corresponding elevations levels estimated by employing the QPS technique in Figure 6 closely fit the actual levels on the ground. In addition, since the downriver part of the dam is in the line of sight of the satellite, the elevation of the left of the dam can be represented as three parts: the elevations of the tail water platform, the top of the plant house, and the top of the dam. The elevation of the lifting equipment on top of the dam was measured to be about 200 m. Five levels of the permanent ship locks, although there are not so many QPS points, can also be observed. The

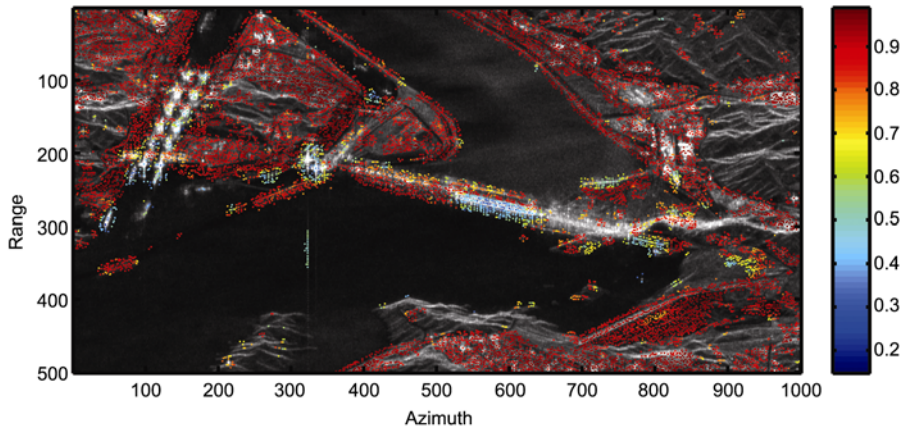

Figure 5 Temporal coherence obtained by employing the QPS technique. The background is the amplitude mean values of processed SAR images.

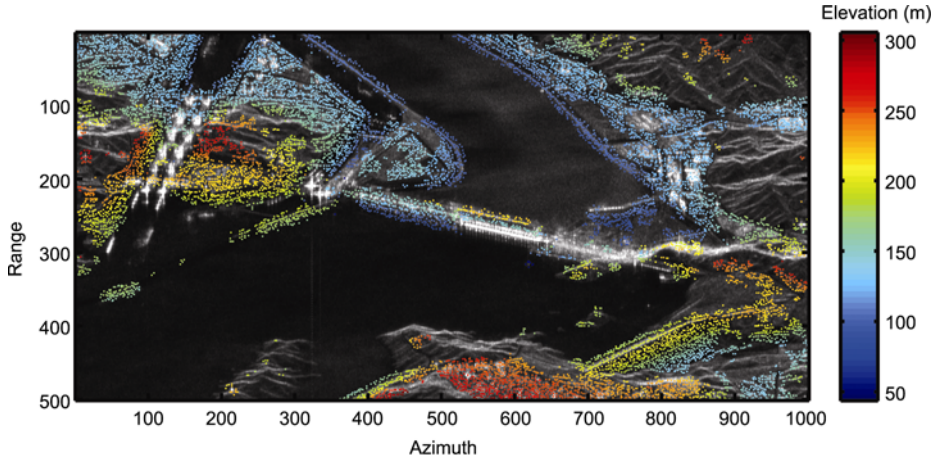

Figure 6 Measured elevation of QPSs. The threshold to select a QPS is 0.75.

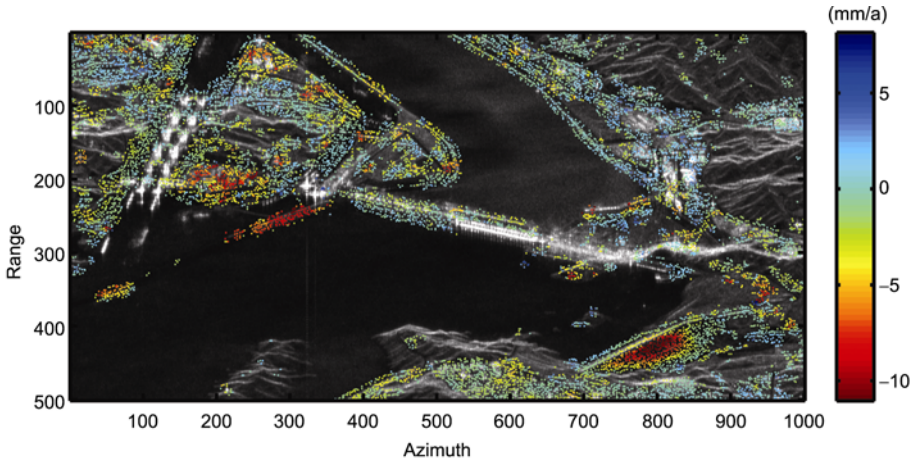

Figure 7 Measured deformation for QPSs. The threshold to select a QPS is 0.75.

above analysis indicates that the elevation measured by employing the QPS technique is reliable and can be used as the initial height values for PS analysis.

The trends of deformation measured by employing the QPS technique are shown in Figure 7. Since the interferograms obtained by employing the QPS technique usually have short temporal baselines, the accuracy of the deformation measurements is low. Nevertheless, the trends of the deformation estimates show that the theoretical accuracy still can reach 1 mm/a.

Figure 7 shows that there are only slight deformation trends around the dam; i.e., the Three Gorges Dam is quite

stable during the time span of our dataset. There are three types of deformation of a dam [42]: 1) deformation related to water pressure, 2) deformation related to temperature and 3) temporal subsidence. The deformation related to water pressure is caused by the pressure of the upriver reservoir acting in downward and downriver directions, the deformation related to temperature is caused by thermal dilation, and the temporal subsidence is caused by pressure over the earth crust due to the newly built dam. Since the left part of the Three Gorges Dam was completed in 2003, the temporal subsidence caused by the weight of the dam has ceased, and the basin of the dam has become stable [36]. Moreover, it is impossible to determine the deformation related to temperature from the velocity of the deformation. Therefore, we only analyze deformation related to water pressure using the QPS results.

As shown in Figure 8, there are three types of deformations related to water pressure: 1) the upriver reservoir presses the earth crust and inclines the basement of the dam, and thus, the dam is inclined in the upriver direction, 2) the upriver reservoir pushes the dam in the downriver direction and 3) there is flexing deformation due to upriver pressure and all are shown in Figure 8(a)–(c), respectively. Figure shows that on the top of the left part of the dam, the slight deformation trends are away from the satellite, whereas the plant houses at the base of the dam have deformation trends toward the satellite. We presume that the dam declined slightly on account of the upriver water pressure over the riverbed crust during 2003–2008, and this is the main reason for deformation of the Three Gorges Dam. However, the factors of dam deformation are complicated; thus, it is difficult to interpret the displacement of the dam only from the deformation trends. In the following discussions, we also consider the time series phases from PS processing in analyzing the deformation pattern of the dam.

For the dam surroundings, we detected several subsidence areas on the left riverbank, especially along the axis of the dam to the area between the ship lift and permanent ship locks. We presume that construction of the navigation establishments changed the distribution of the underground water and caused surficial subsidence. In addition, several areas of slight subsidence are observed near the Yangtze. According to Figure 7, synthetically, there was frequent surficial subsidence near the water area of the Yangtze and the subsidence is greatest on the upriver embankment near Zigui County. The highest subsidence velocity exceeds 10 mm/a, and we highlight the observed phenomenon for consideration by the local government.

Using the QPS processing results, PS analysis was carried out with the same dataset. Since the PS technique can precisely measure deformation for PS targets from the residual phases, the deformation of the dam can be analyzed by considering the effects of the water level and temperature. In the QPS process, we set 0.75 as the threshold for selecting a PS; however, only about 2000 PSs are detected, most of which are on artificial targets such as the dam and the ship lock lookout.

From the QPS results, we presume that the temporal subsidence of the dam almost ceased after construction of the concrete building. Therefore, water pressure and temperature are the main factors for the deformation of the dam. Figure 9(a) and (b) show the time-series residual phases of two PSs on the dam. Figure 9(a) relates to a target on top of the dam and (b) to a target on the tail water platform. Figure 9(c) and (d) show the upriver-downriver water level difference and upriver water level respectively for the duration of data acquisition[2)], from which, similar trends can be observed. The three red dashed lines in Figure 9 indicate the

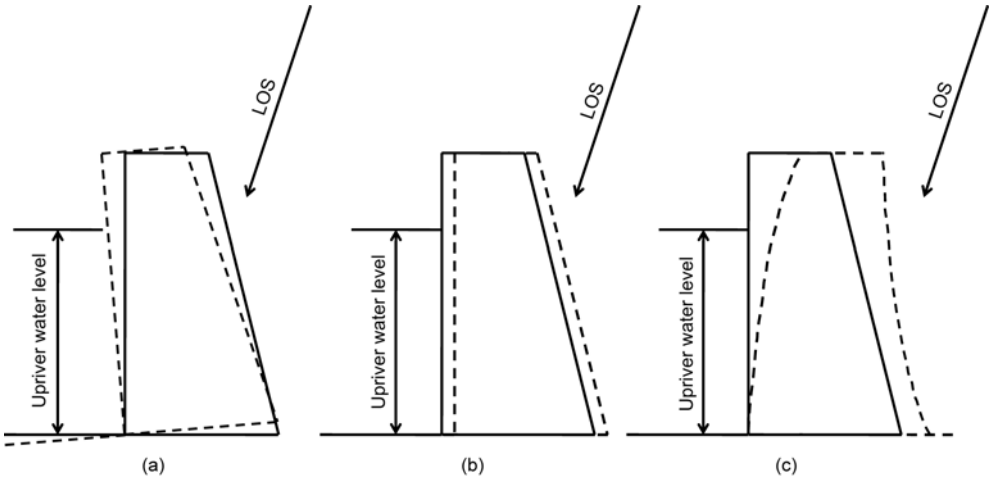

Figure 8 Three types of dam deformation caused by the pressure of water. The arrow indicates the radar line of sight. (a) The upriver reservoir presses the earth crust and inclines the basement of the dam; thus, the dam is inclined in the upriver direction. (b) The upriver reservoir pushes the dam in the downriver direction. (c) Flexibility deformation due to horizontal upriver pressure.

2) The hydrologic data were acquired from the website of the Three Gorges Project Corporation (http://www.ctgpc.com.cn).

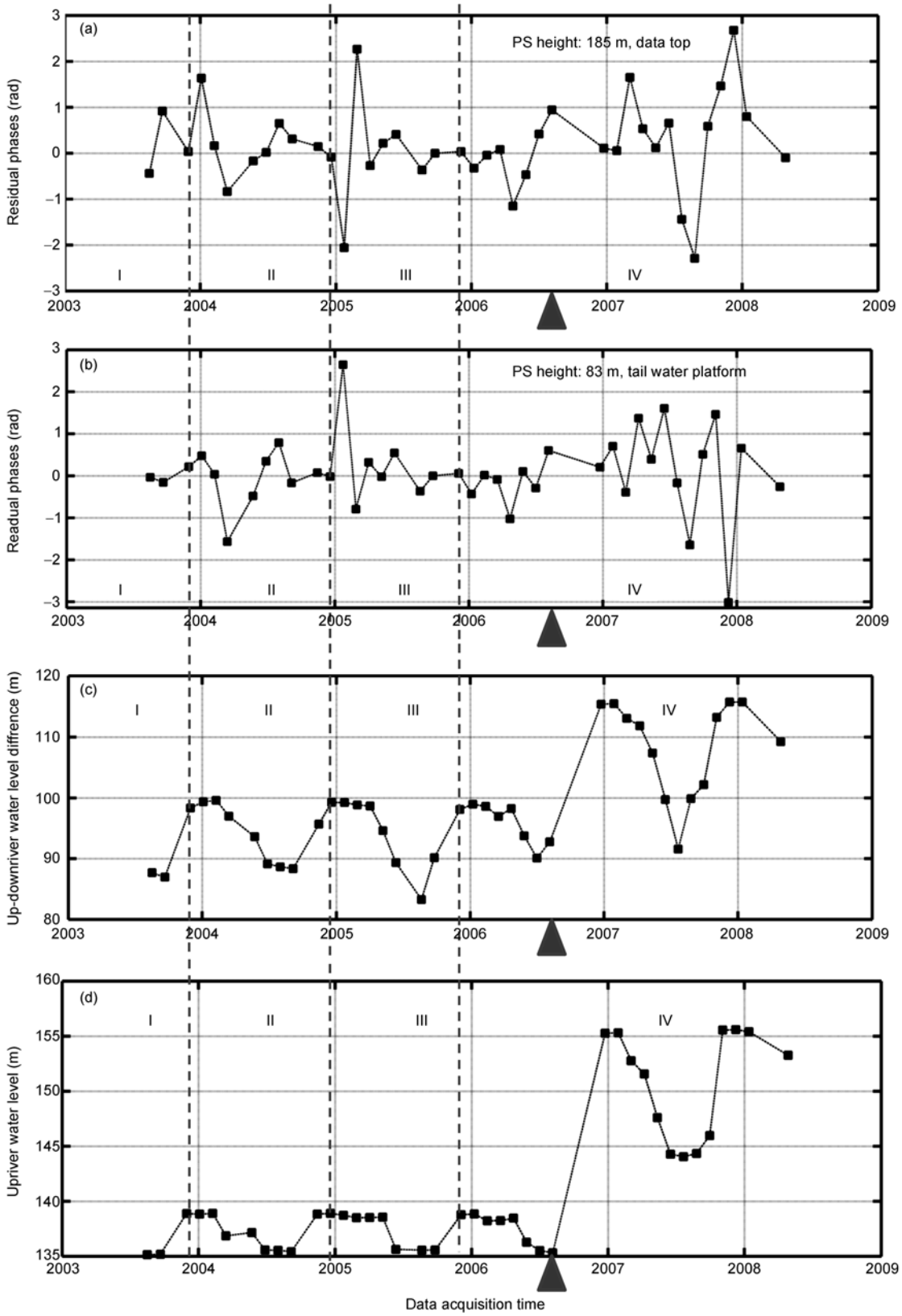

Figure 9 Relations between residual phases for PSs and the water level. The horizontal axis indicates the data acquisition time. (a), (b) represent the residual phases of two typical PSs at the top and bottom of the left part of the dam. The vertical axis indicates the residual phases; one radian represents 4.5 mm deformation. The vertical axis in (c) indicates the water level difference between upriver and downriver. The vertical axis in (d) indicates the upriver water level. The three red dashed lines indicate the time when the water level difference peaked, and the data acquisition time span is divided into four as indicated by the Roman numbers. The red triangle indicates the time when the cofferdam was dismantled.

times when the upriver-downriver water level difference reached local maximum values, and they divide the time span into four parts denoted I–IV. The red triangle shows the time point of the demolition blasting of the cofferdam.

As indicated by the PS residual phases, when the upriver rose to its highest levels during time spans I–III, remarkable deformation was detected when employing the PS technique. After the dam had been operational for several months, the deformation trend became relatively consistent. After the cofferdam was dismantled in June 2006 and the Three Gorges Dam first tested while running at a water level of 156 m, the stability reduced, and fluctuating deformation was observed in the PS results. In addition, seasonal deformation caused by thermal dilation was observed at each stable period. According to Figures 9(a) and (b), the deformation values for the top of the dam are larger than those at the base. Our result agrees with the theory that the effect of temperature is greater at the top of the dam than the base [42].

By modeling the QPS and PS measurements from 2003 to 2008, we presume that the left part of the Three Gorges Dam declined slightly upriver on account of the upriver water pressure over the riverbed crust. The temporal subsidence of the dam has since ceased and only slight deformation due to different water levels and temperatures were detected. To validate our results, we referred to a published study that drew two conclusions from long-term deformation measurements of the Three Gorges Dam, considering only the same period as for SAR acquisition [36]. They were: 1) In terms of vertical deformation, the subsidence of the dam basement has ceased and there has been some rebound. 2) In terms of horizontal deformation, although the dam basin is very stable, there is displacement of the dam in the upriver direction at 175 m elevation. Clearly, the results closely fit our measurements by employing time-series InSAR analysis.

3.3 Interpretation of results for areas of low temporal coherence

Figure 5 shows that areas of low coherence are mainly in the middle and right parts of the dam and navigational establishments. Because the ship locks open and close when a ship passes through, the temporal coherence is greatly reduced, even for the selected interferometry-image subset. There are only a few PS candidates (PSCs) for the plant houses on the right side of the dam, since it was under construction during the time of data acquisition. Nevertheless, the topography and deformation were still measured for the cofferdam. Moreover, some QPSs are detected on top of the spillway and the navigation establishments. The results demonstrate the adaptability of the QPS technique in complicated situations.

Although there are many PSCs on the spillway, their estimated temporal coherence was very low. From amplitude analysis over the 40 SAR images, we find that there are two states for the spillway, namely the states of releasing and storing water. When the sluice gates are open, the released water scatters the radar signal and a very low amplitude is observed in the corresponding SAR image. This problem can explain the low temporal coherence we observed when employing the QPS technique. The logarithm mean amplitude maps for the two different states are shown in Figure 10(a) and (b). In Figure 10(c), the difference between (a) and (b), focusing on the spillway, is shown, from which even individual sluice gates can be observed owing to their different reflective characteristics in different states. In the case of mid-resolution SAR images, it is difficult to determine structural details on such a scale. The number of images acquired when the gates are closed is insufficient to carry out a reliable time series analysis, and thus we could not obtain the deformation for the sluice gates. However, time-series InSAR analysis along with the archiving of data and collection of high-resolution SAR images will allow measurement of the deformation for the right plant house and spillway of the dam.

4 Conclusions

In this work, we present time-series InSAR analysis by employing PS and QPS techniques. Our results demonstrate the feasibility of deformation monitoring using time-series SAR images and we present measurements of the elevation and deformation over the area of the Three Gorges Dam. Compared with conventional survey methods, the benefits that can be gained from the time-series InSAR dataset are as follows. 1) Field work and a monitoring station are not needed. If necessary, corner reflectors can be installed within the dam site to improve the accuracy of the measurements; nevertheless, our results demonstrate that corner reflectors are not a requirement. 2) The coverage of SAR images allows us to monitor the deformation on a large scale. For example, one ESA SAR image can cover an area of 100 km×100 km; thus, the whole upriver reservoir can be monitored with only 7–8 tracks images. On such a scale, we can measure not only the deformation of the dam, but also the geologic deformation along the river (e.g., we have obtained the deformation around Badong [35]). 3) The density of observation points collected by employing the PS-InSAR technique is much higher than that in conventional survey methods; over the dam site, we can obtain tens and even hundreds of PSs and QPSs per square kilometer.

Time-series InSAR analysis allows us to extract precise geometric parameters using remote sensing data. The density and coverage of the measurement points can be much higher than conventional survey methods. For example, although the differential GPS technique can obtain millimeter-level deformation monitoring results, the measurement number and coverage area usually cannot be guaranteed. If

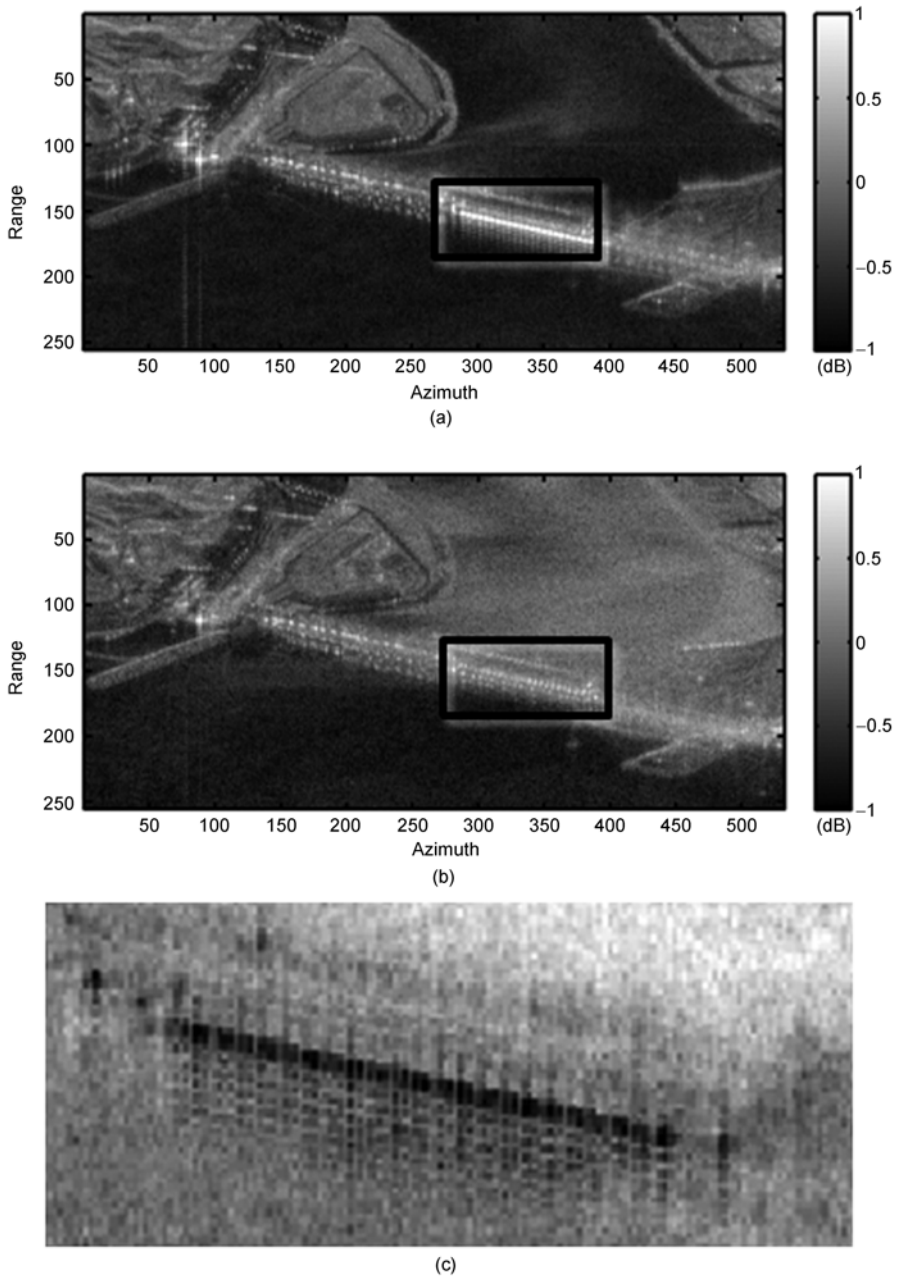

Figure 10 Logarithm mean amplitude maps when the spillway was open and closed, and their difference. The spillway is indicated by the black rectangle. (a) The spillway is closed. (b) The spillway is open. (c) Enlarged portion of the differential image between (a) and (b).

we use the precise measurements from GPS to model the deformation pattern in the time-series InSAR analysis, the measurement accuracy as well as the density and coverage of the monitoring points can be significantly improved. The combination of the two deformation measurement methods allows us to monitor the deformation with acceptable expense and identify areas of abnormal deformation in time for appropriate action to be taken. Recently, new-generation satellites with higher resolution and shorter revisiting times have been launched, and thus the accuracy of monitoring deformation from time-series SAR images will be improved further [43, 44]. Therefore, along with conventional survey methods such as GPS and leveling methods, high-accuracy and high-density dam stability monitoring results can be expected.

This *work was supported by National Basic Research Program of China (Grant Nos. 2007CB714405, 2006CB701300), National Natural Science Foundation of China (Grant No. 40721001) and Three Gorges Region Geologic Disaster Protection Major Research Program (Grant No. SXKY3-6-4).*

1 Li Q, Zhao X, Cai J A, et al. P wave velocity structure of upper and middle crust beneath the Three Gorges reservoir dam and adjacent

regions. Sci China Ser D-Earth Sci, 2009, 52: 567–578
2 Fourniadis I G, Liu J G, Mason P J. Regional assessment of landslide impact in the three gorges area, China, using ASTER data: Wushan-Zigui. Landslides, 2007, 4: 267–278
3 Shen C, Sun S, Liu S, et al. Dynamic variations of gravity field in head area of Three Gorges reservoir in recent years (in Chinese). J Geod Geodyn, 2004, 24: 6–13
4 Yang J, Wu Z. Present conditions and development of dam safety monitoring and control researches home and abroad (in Chinese). J Xi'an Univ Technol, 2002, 18: 26–30
5 Yan J, Li S. Optimization design of deformation monitoring for TGP's dam (in Chinese). Yangtze River, 2002, 33: 36–38
6 Li Z, Liu Z, Wang Z. GPS in dam deformation monitoring (in Chinese). J Wuhan Univ Hydraulic Electr Eng, 1996, 29: 26–29
7 Guo H. Theory and Application of Earth Observation with Radar (in Chinese). Beijing: Science Press, 2000
8 Liao M, Lin H. Synthetic Aperture Radar Interferometry—Principle and Signal Processing (in Chinese). Beijing: Survey Press, 2003
9 Rosen P A, Hensley S, Joughin I R, et al. Synthetic aperture radar interferometry. Proc IEEE, 2000, 88: 333–382
10 Hanssen R F. Radar Interferometry Data Interpretation and Error Analysis. Dordrecht: Kluwer Academic Publishers, 2001
11 Madsen S, Zebker H, Martin J. Topographic mapping using radar interferometry: Processing techniques. IEEE Trans Geosci Remote Sens, 1993, 31: 246–256
12 Liao M, Wang T, Lu L, et al. Reconstruction of DEMs from ERS-1/2 tandem data in mountainous area facilitated by SRTM data. IEEE Trans Geosci Remote Sens, 2007, 45: 2325–2335
13 Gabriel A K, Goldstein R M, Zebker H A. Mapping small elevation changes over large areas: Differential radar interferometry. J Geophys Res, 1989, 94: 9183–9191
14 Wang C, Zhang H, Shan X, et al. Application SAR interferometry for ground deformation detection in China. Photogramm Eng Remote Sens, 2004, 70: 1157–1166
15 Ge, L, Chang H, Rizos C. Mine subsidence monitoring ssing multi-source satellite SAR images. Photogramm Eng Remote Sens, 2007, 73: 259–266
16 Zebker H. On the derivation of coseismic displacement fields using differential radar interferometry: The landers earthquake. J Geophys Res, 1994, 99: 19617–19634
17 Shan X J, Ma J, Wang C L, et al. Co-seismic ground deformation and source parameters of Mani *M*7.9 earthquake inferred from spaceborne D-InSAR observation data. Sci China Ser D-Earth Sci, 2004, 47: 481–488
18 Zebker H, Villasenor A J. Decorrelation in interferometric radar echoes. IEEE Trans Geosci Remote Sens, 1992, 30: 950–959
19 Goldstein R. Atmospheric limitations to repeat-pass interferometry. Geophys Res Lett, 1995, 22: 2517–2520
20 Ding X, Li Z, Zhu J, et al. Atmospheric effects on InSAR measurements and their mitigations. Sensors, 2008, 8: 5426–5448
21 Ferretti A, Prati C, Rocca F. Permanent scatterers in SAR interferometry. IEEE Trans Geosci Remote Sens, 2001, 39: 8–20
22 Ferretti A, Prati C, Rocca F. Nonlinear subsidence rate estimation using permanent scatterers in differential SAR interferometry. IEEE Trans Geosci Remote Sens, 2000, 38: 2202–2212
23 Colesanti C, Ferretti A, Novali F, et al. SAR monitoring of progressive and seasonal ground deformation using the permanent scatterers technique. IEEE Trans Geosci Remote Sens, 2003, 41: 1685–1701
24 Perissin D, Prati C, Engdahl M E, et al. Validating the SAR wavenumber shift principle with the ERS Envisat PS coherent combination. IEEE Trans Geosci Remote Sens, 2006, 44: 2343–2351
25 Ferretti A, Savio G, Barzaghi R, et al. Submillimeter accuracy of InSAR time series: Experimental validation. IEEE Trans Geosci Remote Sens, 2007, 45: 1142–1153
26 Perissin D. Validation of the sub-metric accuracy of vertical positioning of PS's in C Band. IEEE Lett Geosci Remote Sens, 2008, 5: 502–506
27 Wang Y, Liao M, Li D, et al. Subsidence velocity retrieval from long term coherent targets in radar interferometric stacks (in Chinese). Chin J Geophys, 2007, 50: 598–604
28 Perissin D, Rocca F. High-accuracy urban DEM using permanent scatterers. IEEE Trans Geosci Remote Sens, 2006, 44: 3338–3347
29 Perissin D, Ferretti A. Urban target recognition by means of repeated spaceborne SAR Images. IEEE Trans Geosci Remote Sens, 2007, 45: 4043–4058
30 Kampes B M. Radar Interferometry Persistent Scatterer Technique. Dordrecht: Springer, 2006.
31 Hooper A, Segall P, Zebker H. Persistent scatterer interferometric synthetic aperture radar for Crustal deformation analysis, with application to Volcán Alcedo, Galápagos. J Geophys Res, 2007, 112: B07407, doi: 10.1029/2006JB004763
32 Mora O, Mallorqui J J, Broquetas A. Linear and nonlinear terrain deformation maps from a reduced set of interferometric SAR images. IEEE Trans Geosci Remote Sens, 2003, 41: 2243–2253
33 Perissin D, Ferretti A, Piantanida R, et al. Repeat-pass SAR interferometry with partially coherent targets. Fringe 2007, Frascati (Italy), 26–30 November, 2007
34 Hilley G, Burgmann R, Ferretti A, et al. Dynamics of slow-moving landslides from permanent scatterer analysis. Science, 2004, 304: 1952–1955
35 Wang T, Perissin D, Liao M, et al. Deformation monitoring by long term D-InSAR Analysis in Three Gorges area, China. Geoscience and Remote Sensing Symposium, IEEE International, 2008
36 Dai H, Su H. Stability against sliding in intake dam section of Yangtze River Three Gorges Project (in Chinese). Rock Soil Mechanics, 2006, 27: 643–647
37 Touzi R, Lopes A, Bruniquel J, et al. Coherence estimation for SAR imagery. IEEE Trans Geosci Remote Sens, 1999, 37: 135–149
38 Biggs N L. Discrete Mathematics. Oxford: Claredon Press, 1985
39 Zebker H, Chen K. Accurate estimation of correlation in InSAR observations. IEEE Lett Geosci Remote Sens, 2005, 2: 124–127
40 Gatelli F, Guamieri A M, Parizzi F, et al. The wavenumber shift in SAR inferometry. IEEE Trans Geosci Remote Sens, 1994, 32: 855–865
41 Liu G. Geology engineering overview of the Three Gorges Project (in Chinese). Hydrogeol Eng Geol, 1993, 20: 56–57
42 Huang S, Yin H, Jiang Z. Deformation Monitoring Data Processing (in Chinese). Wuhan: Wuhan University Press, 2004
43 Liao M, Tian X, Zhao Q. Missions and applications of TerraSAR-X/Tandem-X (in Chinese). J Geomatics, 2007, 32: 44–46
44 Soergel U, Thoennessen U, Brenner A, et al. High-resolution SAR data: New opportunities and challenges for the analysis of urban areas. IEEE Proc Radar Sonar Navigation, 2006, 153: 294–300